Available online at www.sciencedirect.com

ScienceDirect

Procedia Technology 16 (2014) 886 – 896

Procedia Technology

CENTERIS 2014 - Conference on ENTERprise Information Systems / ProjMAN 2014 - International Conference on Project MANagement / HCIST 2014 - International Conference on Health and Social Care Information Systems and Technologies

Multi-temporal InSAR for deformation monitoring of the Granada and Padul faults and the surrounding area (Betic Cordillera, southern Spain)

Joaquim J. Sousa[a,b,*], Antonio M. Ruiz[c,d], Andrew J. Hooper[e], Ramon F. Hanssen[f], Zbigniew Perski[g], Luisa C. Bastos[h,i], Antonio J. Gil[c,d], Jesús Galindo-Zaldívar[j,k], Carlos Sanz de Galdeano[k], Pedro Alfaro[l], Mª Selmira Garrido[c,d], Juan A. Armenteros[c], Elena Giménez[c], Manuel Avilés[c]

[a]*Department of Engineering, School of Science and technology, University of Trás-os-Montes e Alto Douro, Vila Real, Portugal*
[b]*Center of Geology, University of Porto, Portugal*
[c]*Departamento de Ingeniería Cartográfica, Geodésica y Fotogrametría, Universidad de Jaén, Jaén, Spain*
[d]*Centro de Estudios Avanzados en Ciencias de la Tierra (CEACTierra), Universidad de Jaén, Jaén, Spain*
[e]*School of Earth and Environment, The University of Leeds, Leeds, United Kingdom*
[f]*Department of Geoscience and Remote Sensing, Delft University of Technology, Delft, The Netherlands*
[g]*Polish Geological Institute - National Research Institute, Carphatian Branch, Cracow, Poland*
[h]*Observatório Astronómico, Faculdade de Ciência da Universidade do Porto, Portugal*
[i]*Department of Geosciences, Environment and Spatial Planning, Faculty of Science, University of Porto, Portugal*
[j]*Departamento de Geodinámica, Universidad de Granada, Granada, Spain*
[k]*Instituto Andaluz de Ciencias de la Tierra, Consejo Superior de Investigaciones Científicas-Universidad de Granada, Granada, Spain*
[l]*Departamento de Ciencias de la Tierra y Medio Ambiente, Universidad de Alicante, Apdo. 99, San Vicente del Raspeig, Alicante, Spain*

Abstract

The quantification of low rate active tectonic structures is a major target of geodetic and geological studies to improve the knowledge of seismic hazards. The central Betic Cordillera (southern Spain) is affected by moderately active tectonic structures and seismicity. Part of this seismic activity is produced by several NW-SE normal faults located in the E of the Granada Basin.

* Corresponding author. Tel.: +351 259 350 357; fax: +351259 350 356.
E-mail address: jjsousa@utad.pt

Peer-review under responsibility of the Organizing Committee of CENTERIS 2014.
doi:10.1016/j.protcy.2014.10.040

Here, we apply Multi-temporal InSAR (MTI) data to quantify the deformation produced by the Granada fault and the Padul fault zones and the surrounding area. The Granada NW-SE active normal fault zone, 17 km in length, crosses the city of Granada, a very sensitive area from a seismic hazard point of view due to the population of the Granada town. At the Padul fault, there is no geodetic evidence of contemporary motion. Considering the evidence of recent activity from geologic data, this fault may experience discontinuous motion with a different seismogenic character. Despite the InSAR uncertainties, InSAR results are consistent with the estimated geologic deformation rates lower than 1 mm/yr. Our results also confirm previous InSAR studies in the Otura area showing an estimated average annual velocity along the SAR line-of-sight of up to 10 mm/year anthropogenic subsidence.

Peer-review under responsibility of the Organizing Committee of CENTERIS 2014.

Keywords: Granada fault; Padul fault; deformation; persistent scatterers; small baseline; InSAR; StaMPS;

1. Introduction

The Granada metropolitan area (southern Spain), with a population of over 500,000 people, is one of the areas with the highest seismic hazard of the Iberian Peninsula [1]. The most recent destructive earthquake of the Iberian Peninsula occurred in 1884 in the Granada Basin, about 50 km southwest from the city. With felt intensities of IX-X and an assigned macroseismic magnitude in the order of M=6.5, it caused about 800 fatalities. In addition, the Granada Basin experiences the highest seismicity rate of the Iberian Peninsula [2,3,4,5,6], characterized by earthquake swarms [7] and several instrumental earthquakes with magnitudes around 5.0. The most significant event is the 1956 NW Purchil earthquake (mb 5.0, I=VIII), causing 11 deaths. In addition, there is evidence of historical earthquakes in the study area, in the NE of the Granada Basin, such as the 1431 earthquake which produced severe damage in the Alhambra Palace in Granada [8].

Several studies based on geologic and geomorphic markers have estimated moderate slip rates of the main active faults of the area [7]. These studies conclude that most of the active faults of the Granada Basin are normal, with slip rates between 0.06 and 0.5 mm/yr, producing mainly vertical displacements between the fault blocks.

In addition, several researches integrating geologic and geodetic studies were carried out in the study area: for instance, [9] and [10] analyzed the Padul fault area by means of a local triangulation-trilateration network, but no significant movements were detected due to the low fault deformation in the measured period. Furthermore, [10] analyzed the tectonic activity of the Granada fault area, a NW-SE oriented fault zone crossing the city of Granada, surveying two leveling profiles (Víznar and Genil) in 1999, 2000 and 2001, but very low rates of vertical displacement, close to the detection limit of geodetic techniques, were recorded. More leveling surveys have been carried out since 2001 until present revealing the discontinuous activity of this fault.

Between the Granada fault and the Padul fault areas, at the southern part of the Granada metropolitan area, a subsidence bowl was detected and analyzed [11,12,13,14,15] with a deformation rate up to 10 mm/yr. The deformation rates remain stable throughout the time span studied (1993-2006). Two main causes were identified to explain this phenomenon: (1) fast infrastructure development taking place in the outskirts of the village of Otura (new residential areas) leading to soil compaction, and (2) intensive withdrawal of water from underground originated for the increase of population in the last years. The detected subsidence makes the future monitoring of the area of crucial importance. These previous studies where based on Persistent Scatterer Interferometry (PSI).

The objective of this paper is to compare space-based geodetic techniques with geological data in order to estimate accurate fault slip rates of the Granada and the Padul faults zones and the surrounding area (Fig. 1) to assess its recent behavior and to differentiate between anthropogenic and tectonic deformation. In this paper, we applied time series InSAR techniques (StaMPS-MTI; [16]), that combines both Persistent Scatterer (PS) and Small Baseline (SB) approaches to obtain a regional accurate estimation of deformation. It has been shown that these techniques enable measurement of crustal deformation to be achieved with improved accuracy, in the best scenarios, in the order of 1 mm/yr [17] which is helpful for the quantification of deformation processes that cause small strains.

InSAR techniques give a regional overview to detect possible local anthropogenic deformation which could produce a misunderstanding of the tectonic deformation of a region, especially in areas characterized by low fault

slip rates. Geological data provide long term deformation rates. The comparison between both InSAR and geological data provides new support to differentiate free slip and blocked fault surfaces, with related seismogenic character and seismic hazard.

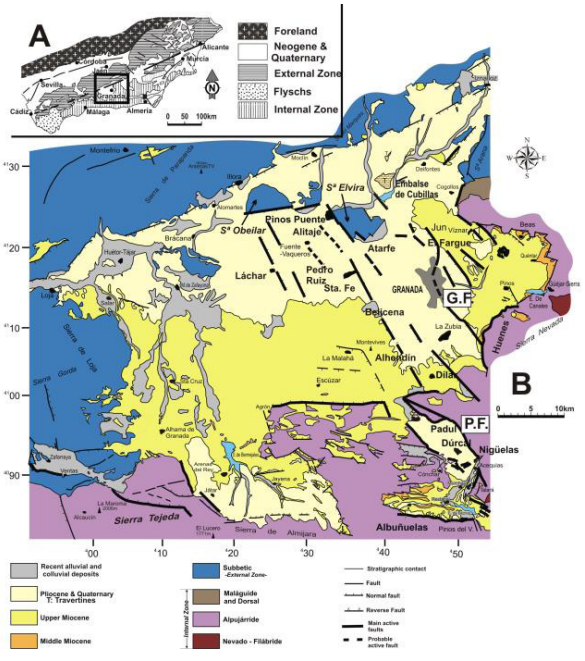

Fig. 1. Geological setting of the study area. (A) Location of the study area in the Betic Cordillera, southern Spain. (B) Simplified geological map of the Granada Basin, including the position of the main NW active normal faults of the NE Granada basin. (G.F.: Granada fault, P.F.: Padul fault). (Adapted from [7]).

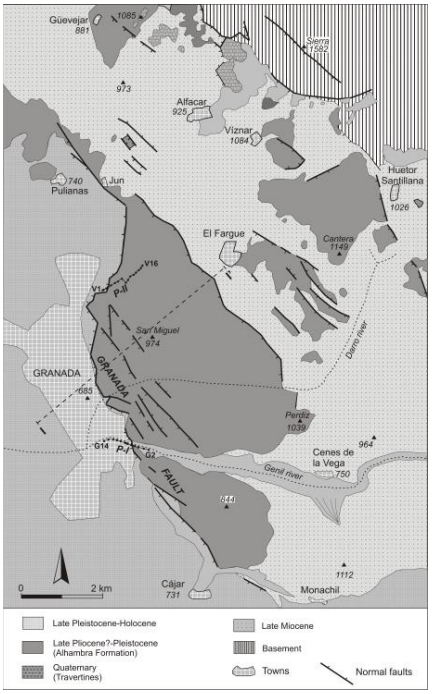

Fig. 2. Geological map of the surroundings of Granada city with location of Granada fault. (P-I: Víznar leveling profile, P-II: Genil leveling profile).

2. Geodynamic setting

Two main areas were selected for applying ground monitoring InSAR techniques: the Granada city area, which includes the Granada fault, and the Padul fault area (Fig. 1). The former area was chosen because it is the most populated city of the central Betic Cordillera and is located in the highest seismic hazard area in the Iberian Peninsula. For these reasons, ground deformation monitoring is crucial in order to mitigate seismic hazards or other natural effects. The Padul fault is located at the west-southwestern termination of the Sierra Nevada, the highest mountain range in the Betic Cordillera, which includes the Mulhacén peak, where the maximum altitude (3482 m) of the entire Iberian Peninsula occurs.

The study area is located in the central Betic Cordillera, in a wide collision zone between the African and Eurasian plates. At present, these plates converge at a rate of approximately 5 mm/yr according to the NUVEL-1A model [18]. From the late Miocene to the present, the Granada Basin is subjected to a NNW-SSE compressive stress field with an associated ENE-WSW tension [19,20]. This tension is accommodated mainly by NW-SE normal faults, most of them, located in the NE and SE sectors of the Granada Basin (Fargue-Jun fault, Granada fault, Sierra Elvira-Dílar fault, Alhendín-Santa Fe fault, Padul fault and Padul-Dúrcal fault, among others), showing geological evidences of recent activity [21,22,23,24,25,26,8,27,28]. This set of NW-SE normal faults, mostly dipping to the southwest, has caused subsidence of several blocks to the west producing topographic steps and fault scarps [29,30,28]. [7] offer a review of the main characteristics of these active faults.

The Granada fault belongs to this set and crosses the city of Granada with a NW-SE to N-S direction (Fig. 2). This is an active normal fault zone measuring ~17 km in length and dipping 60º SW. The fault cuts Pliocene and Pleistocene soft rocks, mainly conglomerates, of the Alhambra Formation [31] proving its recent activity. The fault zone has several splays, roughly parallel to each other, with a total throw of 300 m [7]. This fault zone is characterized by many NW-SE small-scale normal faults dipping 65-75º mostly to the SW, with displacements ranging between a few centimeters and ten meters [30].

Fig. 3. Padul fault aerial photograph at Dúrcal area (courtesy from Javier Sanz de Galdeano).

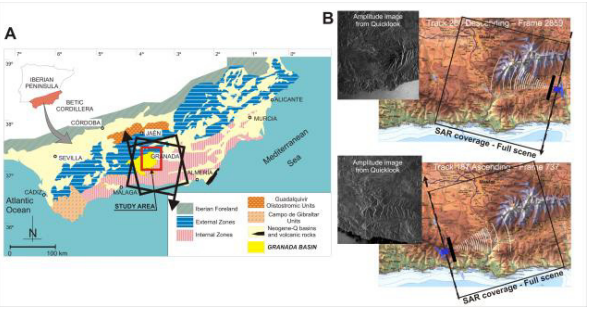

Fig. 4. (A) Simplified geological map of the Betic Cordillera (southern Spain) with location of the study area in the Granada Basin area (small red box) and frames (SAR scenes) used in the study (black rotated boxes), indicating with an arrow the ascending/descending satellite passes (tracks). (B) SAR coverage for both ascending/descending frames.

[7] estimate a fault slip rate of 0.12 mm/yr. The maximum magnitude earthquake for this fault, considering the fault length, is estimated between Mw 6.3 and 6.7 and the reference earthquake has a Mw > 4.9 [7]. Although the area has historical and instrumental earthquakes, it is not possible to associate them with a specific fault due to the depth of seismicity that generally occur around 10 km depth and the presence of several active faults.

The Padul fault also belongs to this system of NW-SE trending normal faults mainly dipping towards the SW. These faults are often associated to asymmetric basins filled with sedimentary wedges of Tortonian and younger ages [32]. The fault is located at the west-southwesternmost termination of the Sierra Nevada and is approximately 12 km long (Fig. 3) with an average NW-SE strike and has various segments which dip towards the SW and S. It consists of two connected segments showing clear evidence of recent activity as a seismic source [8]. In detail, the fault geometry is quite complex and display both low and high angle surfaces; furthermore, there is evidence of progressive rotation of the fault during its evolutionary history [8]. The cumulative vertical displacement associated to the Padul fault is greater than 800 m [23].

Seismic activity along the Padul fault is very scarce. In the period 1980 – 1996, only one earthquake of a magnitude greater than 3 occurred [8]. Despite the low seismic activity, there is abundant geological evidence for the recent activity of this fault [8].

3. InSAR data

Granada Basin and its surroundings (Fig. 4A) are covered by a total of 29 ERS-1/2 SAR scenes from descending satellite track 280 and frame 2859 (Figs. 4B and 5A), and 30 Envisat ASAR scenes from ascending satellite track 187 and frame 729 (Figs. 4B and 5B). The SAR images span the period from December 1993 to October 1999, and between October 2002 and February 2010, respectively for ERS1/2 and Envisat.

A Shuttle Radar Topography Mission (SRTM) C-band DEM with resolution of 3 arc-second geographic resolution (90 m) and 10 meter height accuracy was used as an external DEM to remove the topographic phase from the differential interferograms. Precise orbits data for ERS-1/2 and Envisat satellites, which enable the removal of flat-earth phase from the differential interferograms, were provided by Delft Institute for Earth observation and Space Systems (DEOS) [33].

3.1. Multi-temporal InSAR

Multi-temporal InSAR methods are extensions of conventional InSAR techniques, which address the problems of decorrelation and atmospheric delay by analyzing only pixels that retain some degree of correlation, defined as persistent scatterers (PS). These techniques involve the simultaneous processing of multiple SAR acquisitions over the same area to allow for the correction of uncorrelated phase noise terms and hence, reduce errors associated with the deformation estimates. Currently, multi-temporal InSAR algorithms can be broadly classified into two categories - persistent scatterer (PS) (e.g., [34,35,36]) and small baseline (SB) (e.g., [37,38,39,40]) methods. Each of these set of methods is designed for a specific type of scattering mechanism: point-like and distributed scatterers, respectively for PS and SB methods (for more details on scattering mechanism refer to e.g., [41]).

Stanford Method for Persistent Scatterers - Multi-Temporal InSAR (StaMPS-MTI) combines both PS and SB methods allowing the identification of scatterers that dominate the scattering from the resolution cell (PS) and slowly-decorrelating filtered phase (SDFP) pixels. Finally, the two datasets (PS+SDFP) are combined and further processing is performed on the combined dataset to isolate the deformation signal, based on these stable points (SP). The phase is unwrapped using a 3D approach that utilizes an algorithm developed for regularly gridded data. First, the sparse phase measurements are resampled to a grid using a nearest-neighbor interpolation routine. Then, the optimization routines of SNAPHU [42] are applied.

We based our work on this method, in which assumptions are made about the statistical behavior of the several phase contributions superimposing the deformation term. One of the basic ideas of this method is to assess the temporal stability of the radar targets directly from the interferometric phase. However, since the term representing phase noise is masked by several other terms like atmosphere or phase due to orbital inaccuracies, StaMPS uses an elaborate filtering procedure to remove all these undesired phase contributions. Within this filtering procedure the deformation is modeled to be spatially correlated.

The different steps involved in the StaMPS-MTI processing chain are described in detail in [16,35,43,14,15].

3.2. MTI results

The StaMPS-MTI method was applied to the two datasets presented in Section 3. 28 and 29 interferograms, respectively for ERS-1/2 and Envisat datasets, were used to identify persistent and coherent pixels against 83 and 104 (ERS-1/2 and Envisat, respectively) when applied SB approach (Fig. 5).

Fig. 6 shows the MTI results (PS+SB) over the study area. All the stable points displayed have coherence (a measure of the goodness of fit of the model to the observations, ranging from a minimum of 0 to a maximum of 1) above 0.65. For each stable point, the (mean) Line-Of-Sight (LOS) velocity and the displacement temporal series were computed relative to a circular reference area (radius 2 km) considered stable and marked with the green star in Fig. 6. For the entire datasets, the mean LOS velocity in relation to the reference area falls in the interval -10.3 mm/yr to 2.1 mm/yr. Despite the different temporal reference and different geometries induced by descending (ERS) vs. ascending (Envisat) orbits between both datasets, the general deformation pattern over the processed crop matches well. In particular, it can be seen that the subsidence rates detected in the area reveals the same deformation pattern and maintains the subsidence in both datasets.

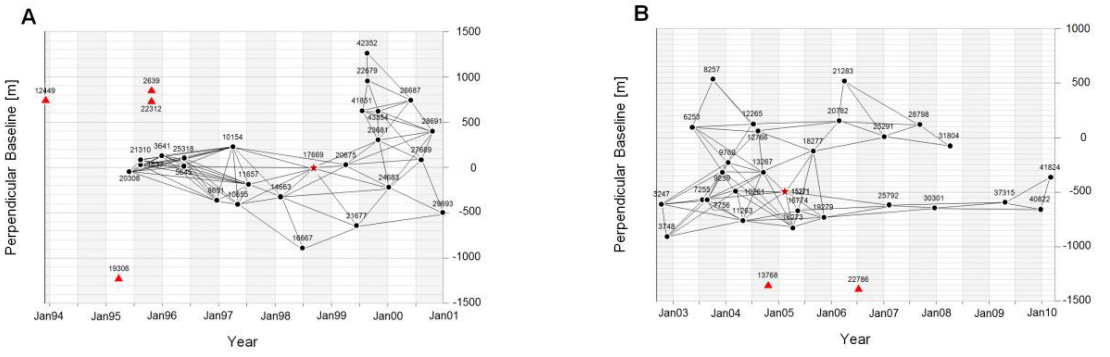

Fig. 5. Temporal vs. spatial baseline distributions for the two interferometric stacks used in this study. The reference scene used in the PS processing is indicated by the start. Black lines indicate the interferograms used in the SB processing and the red triangles represent the scenes not used in the SB processing (spatial baseline > defined parameter). (A) ERS-1/2 descending track. (B) Envisat ascending track.

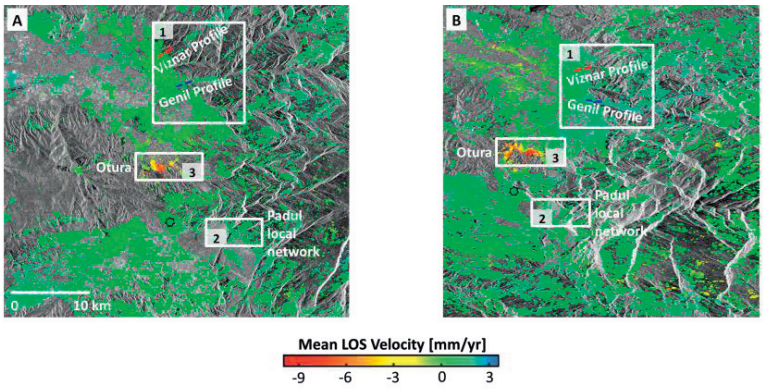

Fig. 6. StaMPS-MTI mean LOS velocity for ERS-1/2 (A) and Envisat (B) stacks. A mean amplitude image is used as a background. The reference area is indicated by a green start. The three areas marked with a white box represent the studied zones (1 - Granada fault, 2 - Padul fault and 3 - Otura village) and are enlarged in Figs. 8, 11 and 10.

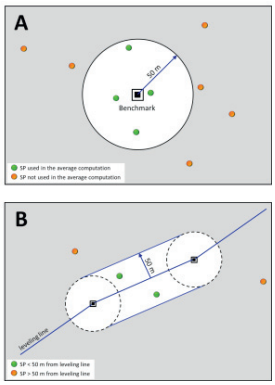

Fig. 7. Stable points selecting criteria for both Genil and Víznar leveling profiles. In the case of Genil benchmarks (A), all the stable points that lie at distance less than 50 m. For Víznar (B), all the stable points located inside a buffer area with maximum distance of 50 m from the leveling line.

4. Discussion: comparison between MTI and geological data

The Granada Basin combines sectors affected by tectonic (Víznar profile of the Granada fault) and anthropogenic deformation (Otura area, intensive water withdrawal). Therefore, accurate fault slip rates must consider the effect of anthropogenic deformation, especially in this study area with very low or discontinuous fault slip rates (between 0.06 and 0.5 mm/yr according to [7]; and 0.12 mm/yr for the Granada fault). To enable the comparison of leveling with MTI results, the mean annual vertical displacement (mm/yr) has been estimated from the calculated height differences between consecutive benchmarks in both leveling profiles. Finally, we interpolated a portion of the MTI mean velocity map, composed of 1281 stable points, with a kriging technique [44] (Genil leveling profile area). To be able to compare MTI time series with leveling results, we selected the stable points that lie at distance less than 50 meters from each benchmark (Fig. 7A) and averaged their projected velocities to the vertical, taking into consideration the SAR incidence angle of 23º. In the Víznar leveling profile area, due to the insufficient amount of detected stable points, we used all the stable points located inside a buffer area with maximum distance of 50 m from the leveling line (Fig. 7B).

Comparing both independent datasets (different sensors, geometries and time reference), it is clear that both reveal the same deformation pattern along the two leveling profiles. It is also evident that only few stable points can be detected along the Víznar profile area due to the unfavorable terrain characteristics (relief and land cover) (Fig. 8B for ERS-1/2 and Fig. 8D for Envisat). The picture appears to be completely distinct in the case of the Genil profile. Each benchmark has more than one stable point within 50 m (Fig. 8C for ERS-1/2 and Fig. 8E for Envisat).

Fig. 9 shows the comparison between MTI and leveling mean velocities (in mm/yr) along the leveling profiles both for ERS and Envisat data processing. The variability of the deformation of these stable points is used to estimate the standard deviation (uncertainty bars in Fig. 9). In general, there is a good agreement between the leveling and MTI results although the discrepancies could be related to the different periods showed for both methodologies. In the case of Víznar line, due to the insufficient amount of detected stable points that lie at distance less than 50 meters for each benchmark, only interpolated and averaged stable points have been computed for benchmark V2. Because of this, in this profile, projected stable points (SP < 50 m leveling line) are shown.

The useful contribution of our MTI results is also shown in the Padul fault (Fig. 6, crop 2), another active normal fault located several km south of the Granada fault, with a slip rate varying between 0.16 and 0.35 mm/yr [7]. No significant deformation was detected by a local triangulation-trilateration network [9,10], which considers a short period of time and a low fault slip rate. In Fig. 11, we can see the StaMPS-MTI results in the area corresponding to the local triangulation-trilateration network (Padul fault). The deformation velocities are in the order of 0 mm/yr.

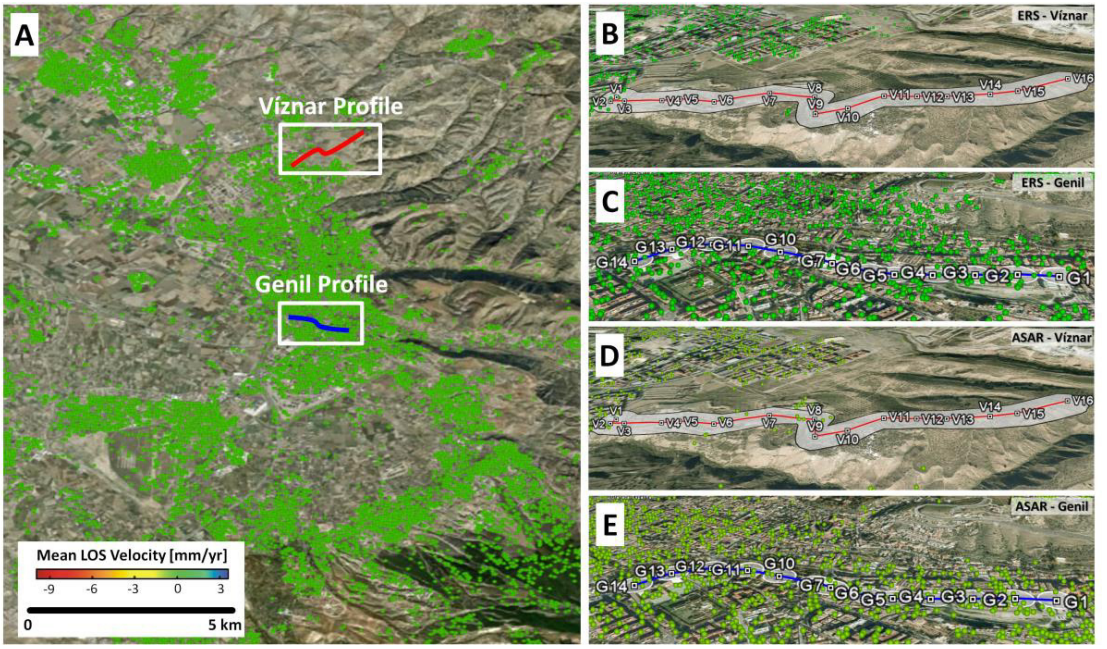

Fig. 8. StaMPS-MTI mean LOS velocity for Granada fault area. (A) Location of Víznar (red line) and Genil (blue line) leveling profiles. (B) and (D) show the results for Víznar profile (ERS-1/2 and Envisat, respectively) as well as the buffer used to select the stable point. (A) and (C) show the results for Genil profile (ERS-1/2 and Envisat respectively) as well as the 50 m radius circles used to select the stable points.

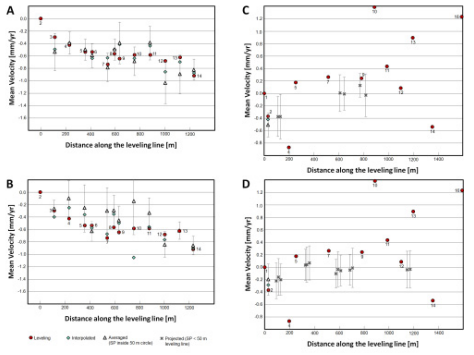

Fig. 9. Leveling and StaMPS-MTI results comparison.
(A) Genil profile – ERS-1/2 1993-1999 vs. Leveling 1999-2011.
(B) Genil profile – Envisat ASAR 2002-2010 vs. Leveling 1999-2011.
(C) Víznar profile – ERS-1/2 1993-1999 vs. Leveling 1999-2009.
(D) Víznar profile – Envisat ASAR 2002-2010 vs. Leveling 1999-2009.
(Interpolated points: stable points selected after interpolation with a Kriging technique along the profile. Averaged points: averaged stable points that lie at distance less than 50 m from each benchmark (Fig. 7A). Projected points: stable points that lie less than 50 m from the leveling line (Fig. 7B)).

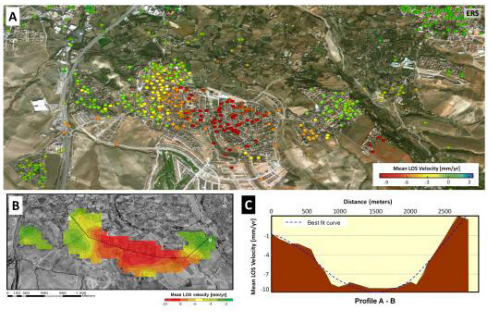

Fig. 10. (A) StaMPS-MTI stable points, with maximum values of 10 mm/yr, distribution over Otura village superimposed to a Google-Earth image where the same color code than for Fig. 6 is used. (B) Color contour intervals for a masked area inside the subsidence bowl superimposed to a 0.5 m resolution ortophoto used as a background. The profile A-B showing the maximum subsidence is presented in (C).

Again, the favorable characteristics of the descending pass can be observed by the amount of stable points detected in the ERS-1/2 stack (Fig. 11B). However, in both cases (ERS-1/2 and Envisat), the amount of stable points (Fig. 11B and 11C) is high enough to allow the comparison with deformation data obtained by [10]. In Fig. 12B, time series plots corresponding to the stable points located near the triangulation-trilateration network marks and detected in both datasets (ERS and Envisat) are shown. The position of the stable points is given in Fig. 12A. It can be concluded, as in [10], that no significant deformation is detected by any geodetic method during the period of analysis. The deformation rate is below the uncertainty threshold of MTI and geodetic techniques that are in the order of 1 mm/yr, although it is not possible to discard that this fault is blocked and may present a high seismic hazard. Considering that geological markers are deformed by this fault zone, a longer monitoring period is needed to determine its seismic behavior.

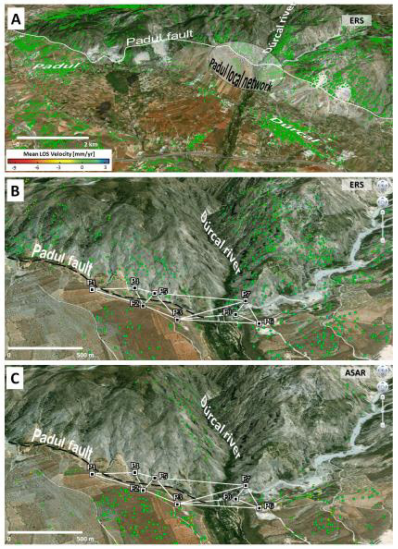

Fig. 11. (A) StaMPS-MTI mean LOS velocity for Padul fault area. (B) and (C) show the triangulation-trilateration network over the Padul fault together with the surrounding area for ERS-1/2 and Envisat datasets, respectively.

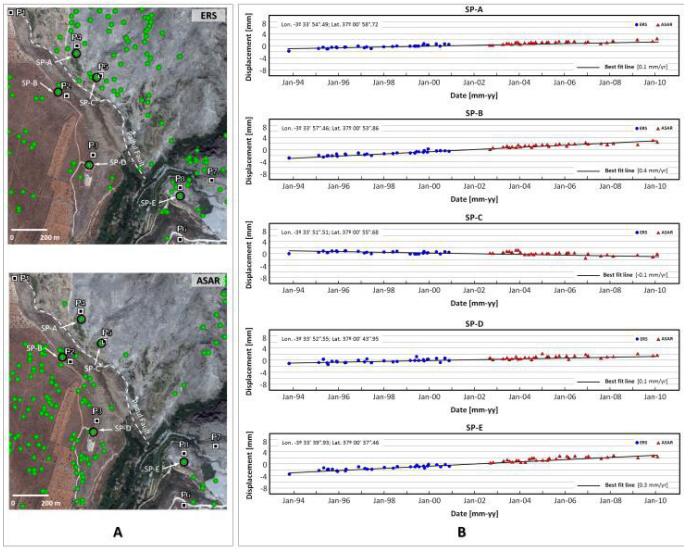

Fig. 12. StaMPS-MTI displacement time series (B) of the selected stable points located nearby some marks of the Padul triangulation-trilateration network (A). These stable points are detected in both datasets (ERS and Envisat).

In addition, this MTI study has also shown the high subsidence area in the village of Otura associated to anthropogenic deformation [11,12,13,14,15] (Fig. 6, crop 3). In Fig. 10, the subsidence pattern for the Otura area, with maximum values of 10 mm/yr, is presented in more detail. Then, considering the absence in the Otura area of outcropping faults and of seismic events, the best possible explanation could be associated to the anthropogenic activity in the sector, with a large expansion of residential building coinciding with a dry period in the region until 1996. These factors determine the increasing of water needs that could have caused a drastic reduction of water table levels of aquifers. As a consequence, the decreases of the saturation of silty and marly silty soft rocks determine a decrease in the rock volume that finally led to high subsidence.

In our study area, E of the Granada Basin, major faults show evidence that tectonic motion in interseismic periods is at least one order of magnitude lower than the observed rates [9,10,7]. Moreover, these MTI studies offer useful information to distinguish anthropogenic deformation and active faults. In the Granada Basin, we clearly identify the areal distribution of anthropogenic deformation, which does not have any relationship with the regional distribution of active faults (Fig. 6). In addition, anthropogenic deformation has an irregular temporal pattern.

5. Conclusions

The application of a MTI approach combining both PS and SB methods (StaMPS-MTI) successfully detected hundreds of thousands of pixels that can be used as monitoring points (stable points). Deformation rates have been monitored during the period 1993-2010. No interseismic deformation has been detected in the E of the Granada Basin, where are located several active structures such as the Granada or Padul faults. Nevertheless, this InSAR study detected a maximum LOS velocity rate of about -10 mm/yr, although it is related to anthropogenic deformation already studied in the Otura village.

The apparent inactivity of the Granada and the Padul faults, however, may be a consequence of the still short monitoring period in respect to the accuracy of the geodetic techniques, or alternatively to an interseismic period of energy accumulation. These faults show clear geological evidence of recent activity and have a high seismic hazard.

The comparison between MTI results and field data further contributes to a validation of the MTI technique. The integration of InSAR with field geodetic techniques and geological data to estimate fault slip rates is highly recommended, to monitoring the different seismogenetic behavior of faults and determining the blocking periods suitable to accumulate elastic energy that is liberated during seismic events. Moreover, the MTI pattern of ground deformation is especially useful to discriminate areas with evidences of anthropogenic from tectonic deformation.

Acknowledgements

SAR data are provided by the European Space Agency (ESA) in the scope of 3858 and 3963 CAT-1 projects. This research was supported by PR2006-0330, ESP2006-28463-E, Consolider–Ingenio 2010 Programme (Topo-Iberia project), CSD2006–0041 (Consolider), AYA2010-15501, P09-RNM-5388, CGL 2006-06001, CGL2010-21048 and CGL2011-30153-C02-02 projects from Ministerio de Ciencia e Innovación (Spain), the RNM-148, RNM-370, RNM-282 and RNM-5388 research groups from the Junta de Andalucía (Spain), and Fundação para a Ciência e a Tecnologia (Portugal). TUDelft radar group are gratefully acknowledged for all the technical support. The SRTM data were provided by USGS/NASA.

References

[1] Comisión Permanente de Normas Sismorresistentes. Norma de construcción sismorresistente: parte general y edificación (NCSR-02). Boletín Oficial del Estado (Spain), 11 de octubre de 2002, nº 244, 35898-35967.

[2] Peláez JA, Sanz de Galdeano C, López Casado C. Use of active fault data versus seismicity data in the evaluation of seismic hazard in the Granada Basin (Southern Spain). Bulletin of the Seismological Society of America 2003; 93:1670-1678.

[3] Sanz de Galdeano C, Pélaez JA, López C. Seismic potentiality of the main faults in the Granada Basin (South of Spain). Pure and Applied Geophysics 2003;160:1537-1556.

[4] Sanz de Galdeano C, Peláez JA. Fallas activas de la Cordillera Bética. Una aproximación a partir de la información tectónica y sísmica. 1st ed. Granada: Editorial Universidad de Granada. 287 pp; 2011.

[5] Morales J, Serrano I, Vidal F, Torcal F. The depth of the earthquake activity in the Central Betics (Southern Spain). Geophysical Research Letters 1997;24:3289-3292.

[6] Serrano I, Zhao D, Morales J. 3-D crustal structure of the extensional Granada Basin in the convergent boundary between the Eurasian and African plates. Tectonophysics 2002;344:61-79.

[7] Sanz de Galdeano C, García-Tortosa FJ, Peláez JA, Alfaro P, Azañón JM, Galindo-Zaldívar J, López-Casado C, López-Garrido AC, Rodríguez-Fernández J, Ruano P. Main active faults in the Granada and Guadix-Baza Basins (Betic Cordillera). Journal of Iberian Geology 2012;38,209-223.

[8] Alfaro P, Galindo-Zaldívar J, Jabaloy A, López-Garrido AC, Sanz de Galdeano C. Evidence for the activity and paleoseismicity of the Padul fault (Betic Cordillera, southern Spain). Acta Geológica Hispánica 2001;36:283-395.

[9] Gil AJ, Rodríguez-Caderot G, Lacy MC, Ruiz AM, Sanz de Galdeano C, Alfaro P. Establishment of a non-permanent GPS network to monitor the recent NE-SW deformation in the Granada Basin (Betic Cordillera, Southern Spain). Studia Geophysica et Geodaetica 2002;46:395-410.

[10] Ruiz AM, Ferhat G, Alfaro P, Sanz de Galdeano C, Lacy MC, Rodríguez-Caderot G, Gil AJ. Geodetic measurement of crustal deformation on NW-SE faults of The Betic Cordillera, Southern Spain, 1999-2001. Journal of Geodynamics 2003;35:259-272.

[11] Sousa J, Hanssen R, Bastos L, Ruiz A, Perski Z, Gil A. Ground Subsidence in the Granada City and Surrounding Area (Spain) using DInSAR Monitoring. In: AGU Meeting 2007, S. Francisco (USA), 10-14 December 2007.

[12] Sousa J, Ruiz A, Hanssen R, Perski Z, Bastos L, Gil A, Galindo-Zaldívar J. PS-InSAR measurement of ground subsidence in Granada area (Betic Cordillera, Spain). In: Proceedings of 13th FIG Deformation Measurement and Analysis, LNEC, Lisbon, 12 – 15 May 2008.

[13] Fernández P, Irigaray C, Jiménez J, Hamdouni R, Crosetto M, Monserrat O, Chacón J. First Delimitation of Areas Affected by Ground Deformations in The Guadalfeo River Valley and Granada Metropolitan Area (Spain) using the DInSAR Technique. Engineering Geology 2009;105:84-101.
[14] Sousa J, Ruiz A, Hanssen R, Bastos L, Gil A, Galindo-Zaldívar J. PS-InSAR processing methodologies in the detection of field surface deformation - study of the Granada Basin (Central Betic Cordilleras, Southern Spain). Journal of Geodynamics 2010;49:181-189.
[15] Sousa J, Hooper A, Hanssen R, Bastos L, Ruiz A. Persistent Scatterer InSAR: A comparison of methodologies based on a model of temporal deformation vs. Spatial correlation selection criteria. Remote Sensing of Environment 2011;115(10):2652-2663.
[16] Hooper A. A multi-temporal InSAR method incorporating both persistent scatterer and small baseline approaches. Geophysical Research Letters 2008;35:L16302.
[17] Hooper A, Bekaert D, Spaans K, Arikan M. Recent advances in SAR interferometry time series analysis for measuring crustal deformation. Tectonophysics 2012;514-517, 1-13.
[18] DeMets C, Gordon RG, Argus DF, Stein S. Effect of recent revisions to the geomagnetic reversal time scale on estimates of current plate motions. Geophysical Research Letters 21;1994:2191-2194.
[19] Galindo-Zaldívar J, Jabaloy A, Serrano I, Morales J, González-Lodeiro F, Torcal F. Recent and present day stresses in the Granada Basin (Betic Cordilleras): example of a late Miocene-present-day extensional basin in a convergent plate boundary. Tectonics 1999;18:686-702.
[20] Herráiz M, De Vicente G, Lindo-Naupari R, Giner J, Simón JL, González-Casado JM, Vadillo O, Rodríguez-Pascua MA, Cicuéndez JI, Casas A, Cabañas L, Rincón P, Cortés AL, Ramírez M, Lucini M. The recent (upper Miocene to Quaternary) and present tectonic stress distributions in the Iberian Peninsula. Tectonics 2000;19:762-786.
[21] Lhénaff R. Néotectonique Quaternairesur le bord occidental de la Sierra Nevada (Province de Grenade, Espagne). Revue de geologie dynamique et de geographie physique 1965;(2),VII,3:205-207.
[22] Estévez A, Sanz de Galdeano C.. Néotectonique du secteur central des Chaînes Bétiques (Basins du Guadix Baza et de Grenade). Revue De Geologie Dynamique Et De Geographie Physique, Paris 1983;21:23-34.
[23] Sanz de Galdeano C. Neotectónica y tectónica activa en el sector Padul-Dúrcal (Borde SW de Sierra Nevada, España). In: Proceedings 1st Conferencia Internacional Sierra Nevada, Granada, Spain, March 1996, p. 219–231.
[24] Keller EA, Sanz de Galdeano C, Chacón J. Tectonic geomorphology and earthquake hazard of Sierra Nevada, South Spain. In: Proceedings 1st Conferencia Internacional Sierra Nevada, Granada, Spain; March 1996, p. 201–218.
[25] Calvache ML, Viseras C, Fernández J. Controls on fan development - evidence from fan morphometry and sedimentology; Sierra Nevada, SE Spain. Geomorphology 1997;21:69-84.
[26] Sanz de Galdeano C, López Garrido AC. Nature and impact of the Neotectonic deformation in the western Sierra Nevada (Spain). Geomorphology 1999;30/3:259-272.
[27] Delgado J, Alfaro P, Galindo J, Jabaloy A, López-Garrido AC, Sanz de Galdeano C. Structure of the Padul-Nigüelas Basins (SE Spain) from H/V ratios of Ambient Noise: Application of the Method to Study Peat and Coarse Sediments. Pure and Applied Geophysics 2002;159:2733-2749.
[28] Rodríguez-Fernández J, Sanz de Galdeano C. Late orogenic intramontane Basin development: the Granada Basin, Betics (southern Spain). Basin Research 2006;18:85-102.
[29] Santanach P, Sanz de Galdeano C, Bousquet JC. Neotectónica de las regiones mediterráneas de España (Cataluña y Cordilleras Béticas). Boletín Geológico Minero de España 1980;91-92:417-440.
[30] Azañón JM, Azor A, Booth-Rea G, Torcal F. Small-scale faulting, topographic steps and seismic ruptures in the Alhambra (Granada, southeast Spain). Journal of Quaternary Science 2004;19:219-227.
[31] Ruiz-Bustos A, Fernández J, Morales J, Rodríguez-Fernández J, Vera JA. Los materiales Plio-Pleistocenos del borde norte de la Depresión de Granada. Estudios Geológicos 1990;46(3/4):277–290.
[32] Galindo-Zaldivar J, Jabaloy A, González-Lodeiro F. Reactivation of the Mecina Detachment in the western sector of Sierra Nevada (Betic Cordilleras, SE Spain). Comptes Rendus de l'Académie des sciences 1996;Série 2,323:615-622.
[33] Scharroo R, Visser P. Precise orbit determination and gravity fleld improvement for the ERS satellites. Journal of Geophysical Research 1998;103(C4):8113-8127.
[34] Ferretti A, Prati C, Rocca F. Permanent Scatters in SAR Interferometry. IEEE Transactions on Geoscience and Remote Sensing 2001;39(1):8-20.
[35] Hooper A, Zebker H, Segall P, Kampes B. A new method for measuring deformation on volcanoes and other natural terrains using InSAR persistent scatterers. Geophysical Research Letters 2004;31:L23611.
[36] Kampes BM. Displacement parameter estimation using permanent scatterer interferometry. Ph.D. Thesis, Delft University of Technology, Delft, Netherlands; 2005.
[37] Lundgren P, Usai S, Sansosti E, Lanari R, Tesauro M, Fornaro G, Berardino P. Modeling surface deformation observed with synthetic aperture radar interferometry at Campi Flegrei caldera. Journal of Geophysical Research 2001;106(B9),19.355–19,366.
[38] Berardino P, Fornaro G, Lanari R, Sansosti E. A new algorithm for surface deformation monitoring based on small baseline differential SAR interferograms. IEEE Transactions on Geoscience and Remote Sensing 2002;40(11):2375-83.
[39] Schmidt DA, Bürgmann R. Time-dependent land uplift and subsidence in the Santa Clara valley, California, from a large interferometric synthetic aperture radar data set. Journal of Geophysical Research 2003;108(B9),2416–2428.
[40] Usai S. A least squares database approach for SAR interferometric data. IEEE Transactions on Geoscience and Remote Sensing 2003;41(4),753–760.
[41] Hooper A. Persistent scatterer radar interferometry for crustal deformation studies and modeling of volcanic deformation, Ph.D. thesis, Stanford University; 2006.

[42] Chen CW. Statistical-cost network-flow approaches to two-dimensional phase unwrapping for radar interferometry. PhD thesis, Stanford University; 2001.
[43] Hooper A, Segall P, Zebker H. Persistent Scatterer InSAR for Crustal Deformation Analysis with Application to Volcán Alcedo, Galápagos, Journal of Geophysical Research 2007;112:B07407.
[44] Press WH, Teukolsky SA, Vetterling WT, Flannery BP. Numerical Recipes: The Art of Scientific Computing (3rd ed.), New York: Cambridge University Press; 2007.